arXiv:1702.05409v1 [cond-mat.mes-hall] 13 Feb 2017

Fabrication and electrical transport properties of embedded graphite microwires in a diamond matrix

J. Barzola-Quiquia,* T. Lühmann, R. Wunderlich,
M. Stiller, M. Zoraghi, J. Meijer, and P. Esquinazi
Institute for Experimental Physics II, University of Leipzig, 04103 Leipzig, Germany

J. Böttner and I. Estrela-Lopis
Institute of Medical Physics and Biophysics,
University of Leipzig, 04107 Leipzig, Germany

(Dated: February 20, 2017)

Abstract

Micrometer width and nanometer thick wires with different shapes were produced ≈ 3 μm below the surface of a diamond crystal using a microbeam of He^+ ions with 1.8 MeV energy. Initial samples are amorphous and after annealing at $T \approx 1475$ K, the wires crystallized into a graphite-like structures, according to confocal Raman spectroscopy measurements. The electrical resistivity at room temperature is only one order of magnitude larger than the in-plane resistivity of highly oriented pyrolytic bulk graphite and shows a small resistivity ratio ($\rho(2\text{K})/\rho(315\text{K}) \approx 1.275$). A small negative magnetoresistance below $T = 200$ K was measured and can be well understood taking spin-dependent scattering processes into account. The used method provides the means to design and produce millimeter to micrometer sized conducting circuits with arbitrary shape embedded in a diamond matrix.

PACS numbers: 81.05.ug, 78.30.Am, 73.63.-b, 61.82.Ms

1. INTRODUCTION

Diamond is a natural allotrope of carbon, transparent, insulating and the hardest natural material on earth. Vavilov and coworkers [1] have shown that it is possible to induce graphitization in diamond by ion irradiation. One of the first works trying to change the transport characteristics of diamond showed that one can produce conducting regions by carbon implantation on the diamond surface [2]. The value and temperature dependence of the resistivity of ion implanted diamond layers was found to be similar to that of amorphous carbon produced by sputtering [2, 3]. In a recently published study, micro-channels were fabricated in single-crystal diamond using a microbeam of He^+ ions in the MeV energy range [4]. The conductivity of the microchannels was improved substantially by annealing treatment, achieving values similar to polycrystalline graphite [4]. The possibility to create a relatively long conducting path of micrometer or even narrower width inside diamond is interesting for possible electrical device applications where the main electronic circuit remains well protected by the highly insulating and biocompatible diamond matrix.

On the other hand, early studies of 100 keV nitrogen and carbon implanted into nano diamonds, show ferromagnetic hysteresis even at room temperature [5], and recent studies on micrometer small areas on single crystal diamond

* Corresponding author: Tel.:+49 341 9732765,E-mail: j.barzola@physik.uni-leipzig.de (Jose Barzola-Quiquia)

after irradiation with 2.2 MeV proton microbeams provided hints on the existence of magnetic order [6, 7]. The authors found that for fluencies below $8.4 \times 10^{17}\text{cm}^{-2}$, a very weak magnetic response was observed at room temperature. In both mentioned studies, the origin of the magnetism was related to the defects produced by the irradiation.

In this work, a similar technique as in Ref. [4] was used to produce conducting microwires beneath the diamond surface using He^+ irradiation. After two annealing steps, different degrees of graphitization of the microwire were reached. Our aim was also to check, whether those conducting structures can show some degree of magnetic order. As was shown in several works in the past, defects like vacancies and/or non-magnetic ions within the graphite structure as well as in a large number of materials, can trigger magnetic order even above room temperature, a phenomenon called defect-induced magnetism (DIM) [8]. Therefore, one can expect that a defective graphitic structure, like the one we produce within the diamond structure by ion irradiation and after annealing, may show some magnetic response. The possibility of having conducting and magnetic microwires within a pure diamond matrix provides a further interesting option for future application.

2. EXPERIMENTAL DETAILS

2.1. Preparation of sub-micrometer width and millimeter long graphite wires

To produce a graphite-like microwire (GLM) inside diamond, we used a polished single crystal (100) diamond of the company Element Six, with a nitrogen concentration < 1 ppm and a boron concentration < 0.05 ppm. The diamond sample was produced by chemical vapor deposition (CVD) with dimension $2.6 \times 2.6 \times 0.3$ mm^3.

The He^+ ion irradiation used to produce the wires in diamond was realized using a very stable high-energy ion nanoprobe in the linear accelerator LIPSION at the University of Leipzig. The wires within the diamond structure was produced with a microbeam of 1.8 MeV energy and an ion current of 2.4 nA.

In our accelerator facilities, using the high-energy ion nanoprobe, we can obtain a sub-micrometer ion beam diameter [9] using a two magnetic quadrupole double lens system. Also, to produce the long size microwire inside the diamond, we need a high ion current and energy stability. This two important conditions are fulfilled with the ion accelerator Singletron$^{\text{TM}}$ from the Dutch company High Voltage Engineering Europa B.V. [10]. The ability to produce complex two dimensional structures (2D) is obtained with the help of a raster unit, which is located between the quadrupole lenses and the sample. Using a self-made program we can produce any desired 2D structure by deflection of the ion beam. According to our experimental conditions, we can continuously deflect the He^+ ion beam within a total area of (1780×1780) μm^2. As examples, using a beam diameter of ≈ 1 μm, a microwire of similar width, see Fig. 1(a), inside a diamond substrate was produced and after annealing, we have graphitized the wire. As a proof of the ability of our ion nanoprobe to produce complex structures (see also other structures in supplementary information), we have prepared a graphitized loop, see Fig. 1 (b-d), which can be used to generate small magnetic fields and/or microwave fields in order to manipulate, e.g., the spin states of NV centers in diamond. The images in Fig. 1 were obtained with a self made confocal optical microscopy implemented with a lens (Olympus MPlanApo 100x/NA0.95), a laser beam with $\lambda = 532$ nm and a lateral and depth resolution of ≈ 300 nm and ≈ 1 μm respectively. Summarizing, we are able to produce long wires with a width of $\approx$ 1 μm and desired shape. These results show the possibilities to produce 2D graphitized structures inside diamond for future applications.

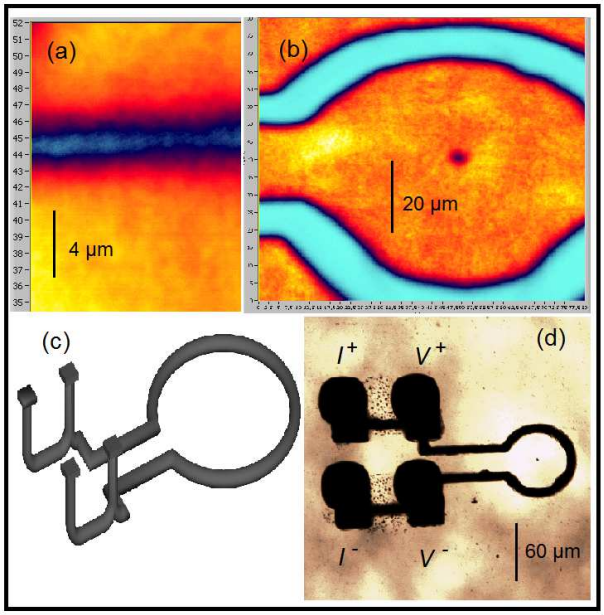

Fig. 1. Image of graphitized structures. (a) Confocal image of a wire with a width in the order of ≈ 1 µm. (b) Confocal image of a wire in shape of a loop. All images taken after annealing (c) 3D sketch of the loop (d) optical picture of the wire loop showing the current-voltage ($I-V$) contacts at the surface of the diamond.

2.2. Irradiation Effects on Diamond and Annealing Treatments

After irradiation of diamond with He^+ ions of energy and fluence similar to the ones we used in this work, an amorphous phase is produced at the region where the irradiated ions stop [1]. By annealing at high temperatures, this amorphous carbon region can later be transformed into graphite or back to diamond structure, which is correlated to the density of vacancies produced by the irradiation. There exists an estimated critical vacancy density $N_{v0} \sim 10^{22}\text{cm}^{-3}$ [11] to induce graphitization in the material after ion irradiation at room temperature and after annealing. According to other experimental work and supported by molecular dynamics simulation, the critical density necessary to graphitize the surface [12] was determined to $N_{v0} \approx 9 \times 10^{22}\text{cm}^{-3}$. Raman measurements indicate that after annealing above $T \approx 700$ K the graphitization process begins by formation and growth of sp^2 bonded nanoclusters [12].

We have irradiated the diamond sample with He^+ ions using a fluence of $\phi = 5.5 \times 10^{17}\text{cm}^{-2}$, which gives a vacancy density $N_v \gtrsim 9\times10^{22}\text{cm}^{-3}$ in a specific depth, see Fig. 2(a) estimated from Monte-Carlo simulation done by SRIM [13]. The program simulates the atomic-displacement cascades in solids on the base of the binary-collision approximation to construct the ion trajectories [14]. For the calculations we have assumed a dislocation energy of 52 eV [15]. This vacancy density is around the minimum value for graphitization after annealing of the ion-produced amorphous carbon phase.

To facilitate the transport measurements performed in this study, the produced GLM had dimension of 15 µm width, 1350 µm total length and a estimated thickness of 130 ± 5 nm, see Fig. 2(a). According to the SRIM calculations the major damage density produced in the diamond sample is located at ≈ 3.1 µm beneath the diamond surface, which was verified by confocal micro-Raman spectroscopy (CRS), see Section 3 3.1.

After He^+ irradiation, the sample was first annealed at $T \approx 1475$ K in a vacuum chamber with a pressure of $P \approx 5 \times 10^{-6}$ mbar (heating rate of 15 K/min and cooling rate of 10 K/min) for 4 hours for the first and for 2 additional hours in the second annealing treatment. After the first and also after the second annealing process the sample was placed in an oxygen plasma chamber at room temperature in order to remove the conducting carbon-based thin layer formed at the surface after the annealing, to avoid any contribution to the transport measurements.

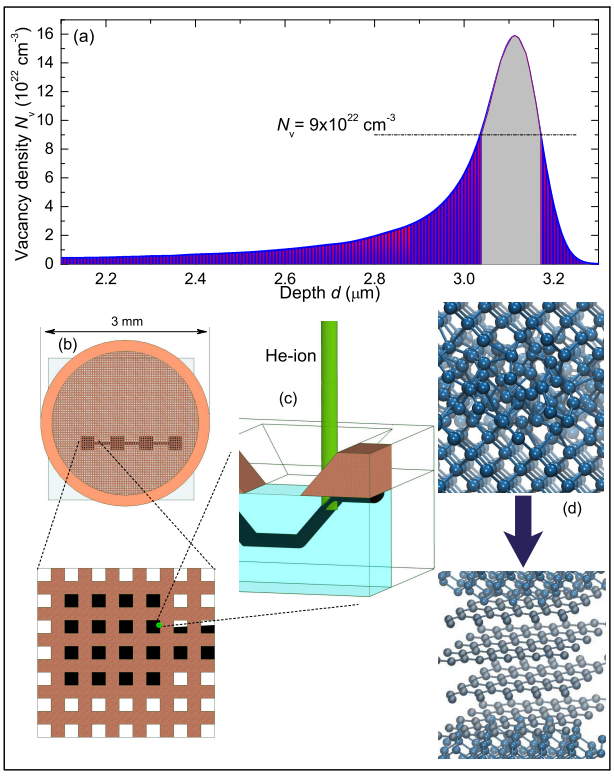

Fig. 2. Sketch of the sample and contact preparation. (a) SRIM simulation showing the vacancy density versus the penetration depth for the fluence and energy (see main text) used in this work. (b) In the first irradiation step, the microwire was produced without a mask, afterwards, the diamond substrate was covered using a copper grid. (c) The sketch shows how contacts from the embedded wire were grown on the substrate surface. (d) Sketch of the amorphous carbon region (top) and the region transformed into graphite (bottom) by annealing at high temperatures.

2.3. Electrical Contacts to the Microwire, Transport and Raman Measurements

The contacts for the electrical measurements have to be done at the surface of the substrate. For this purpose we used a commercial copper grid used for transmission electron microscopy (2000 mesh), having the advantage that the grid has a wedge shape allowing a continuous change of the He^+ ions penetration depth inside the diamond sample, see Fig. 2(b-d). At the surface of the sample and at a distance of $\approx$ 450 μm, square-like contacts with dimension of $\approx 50 \times 50$ μm^2 were prepared in direct electrical contact with the embedded microwire, Fig. 2(c). A similar but more complicated method was already used in Ref. [4]. Afterwards, the electrodes were made by sputtering of Cr/Au directly at the top of the square-like regions at the surface, after an electron beam lithography process. Finally, the contacts to the chip carrier, where the sample was fixed for the transport measurements, were produced using silver paste and gold wires.

Resistance measurements were carried out using the conventional 4-points method using an AC Bridge (Linear Research LR-700) in the temperature range of 2 K to 310 K. For the current-voltage (I–V) measurements, we used the Keithley DC and AC current source (Keithley 6221) and a nanovoltmeter (Keithley 2182). The resistance and its magnetic field dependence were measured with a commercial cryostat from Oxford Instruments with a superconducting solenoid that provides a maximum field of $\pm$ 8 T perpendicular to the main axis of the microwire. Raman characterization was carried out at room temperature using a confocal micro-Raman microscope (alpha300+, WITec company) with an incident Laser light of $\lambda =$ 532 nm, a lateral resolution of $\approx$ 300 nm and axial resolution of $\approx$ 900 nm.

3. RESULTS AND DISCUSSION

3.1. Raman results

To get information about the structural properties of the measured wire produced inside the diamond sample, we have used CRS, which is probably the only method to get information

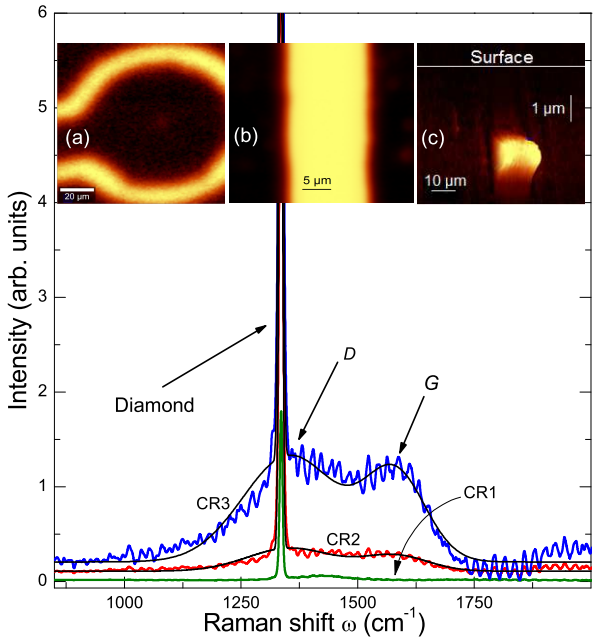

Fig. 3. Raman results measured at the surface and inside the diamond substrate. The curves CR1 and CR3 were obtained fixing the focus of the Raman microscope at the surface (CR1) on the as-received sample, and in a depth of 3 µm (CR3) after irradiation and second annealing. The curve CR2 was obtained from the measurements at the surface after He^+ irradiation and the second heat treatment. The continuous lines through the experimental curves are the fits to the data. The insets show confocal Raman images, in (a) the loop shown in Fig. 1 can be seen, (b) the image shows a close up of a graphite wire and (c) shows an area perpendicular to the surface, i.e. as function of the sample depth. The bright part represents the G-graphite peak.

about the microstructure produced inside the diamond without destroying it. Fig. 3 shows the Raman results.

The curve named CR1 in Fig. 3 was measured at the surface of the as-received diamond sample. The Raman peak at ≈ 1332 cm^{-1} is the characteristic peak for carbon in the diamond structure. The small bump at ≈ 1430 cm^{-1} is related to the appearance of disorder at the surface of the sample during the polish process [16]. The curve CR3 obtained after irradiation and the second annealing was measured with the focus at $\approx$ 3 µm depth from the diamond surface. The results confirm the estimated depth from the SRIM calculations. The results of the curves CR2 and CR3 show three characteristic peaks, one at ≈ 1332 cm^{-1} corresponding to the diamond structure, a second peak due disorder graphite, the so-called D peak at ≈ 1350 cm^{-1}. The third and the most important peak for the characterization of graphite structure, called the G-peak, appears at ≈ 1580 cm^{-1} as a consequence of the double degenerate zone center E_{2g} mode.

Our Raman results resemble those obtained in [12], specially for similar annealing temperatures. The results CR2 and CR3 can be very well fitted using Gaussian functions centered at the aforementioned Raman peaks. The results are shown as continuous black lines in Fig. 3 and describe very well the experimental results. From the fits we get also information about the peak intensity I_G and I_D corresponding to the G and D peak respectively.

From these results it is possible to estimate the crystal size [17] L_a using Eq. (1):

$$L_a(\mathrm{nm}) = (2.4 \times 10^{-10})\lambda_l^4 \left(\frac{I_D}{I_G}\right)^{-1}, \qquad (1)$$

which correlates the crystal size L_a with the integrated intensities of the D and G peaks and the laser excitation wavelength $\lambda_l = 532$ nm. Using this equation, we obtain $L_a = 8 \pm 2$ nm, similar to the results of Rubanov *et.-al.* using transmission electron microscopy [18], where diamond samples were irradiated with He^+ ions using a fluence between $3 \times 10^{16} - 10 \times 10^{16}$cm^{-2} followed by an annealing for 1 h at 1400 °C.

3.2. Temperature Dependence of the Electrical Resistance

After the first annealing the sample shows (at low temperatures) non-linear I–V curves, indicating that non graphitized regions remain in the sample which act like barriers. It has been shown that, whenever a barrier is present between the conducting grains, the resistance $R(T)$ and magnetoresistance (MR) depend on the applied current like in multi-wall carbon nanotubes bundles [19]. Here we do not discuss the $R(T)$ and I–V results after the first annealing (see supplementary information) because our interest lies in the behavior of the transport properties in the Ohmic regime, without any influence of potential barriers, this is obtained after the second annealing treatment.

The resistance results after the second annealing are shown in Fig. 4. The experimental results from 2 K to 315 K are shown as open symbols. The observed temperature dependence is clearly different from the one we obtained after the first annealing treatment. The resistance ratio $R_{A2}(2\mathrm{K})/R_{A2}(315\mathrm{K}) \approx 1.275$ is one order of magnitude smaller than the one after the first annealing, and of the same order as for nano-graphite films [20] and few layer graphene films [21, 22]. The current-voltage curves after second annealing are linear in all measured temperature range and are shown in the supplementary information.

The temperature dependence of the resistance, see Fig. 4, indicates the existence of two different regions, one below and the other above $T \approx 75$ K. We have identified (see supplementary information) that the dominant mechanism at high temperatures is the so-called Mott variable range hopping (VRH) [23], given as:

$$R_{VRH}(T) = R_M \exp\left[\left(\frac{T_0}{T}\right)^{1/4}\right], \qquad (2)$$

where T_0 is a characteristic temperature coefficient defined as:

$$T_0 = \frac{18}{k_{\mathrm{B}}\xi^3 N(E_{\mathrm{F}})}, \qquad (3)$$

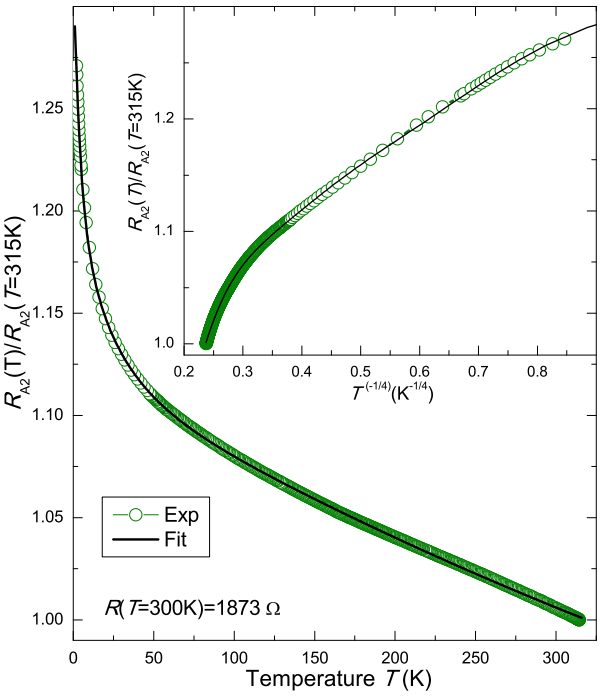

Fig. 4. Temperature dependence of the resistance (after the second annealing). The inset shows the resistance versus $T^{-1/4}$. The continuous lines are the fits results.

and ξ is the localization length, $N(E_{\mathrm{F}})$ the density of states at the Fermi level and R_M is a constant prefactor. In order to fit the resistance over all the measured temperature range, we need to include an extra transport mechanism in parallel (we have also checked other configurations, see supplementary information) given as:

$$R_{A2}(T)^{-1} = R_{VRH}(T)^{-1} + R_m(T)^{-1}, \qquad (4)$$

with

$$R_m(T) = R_0 + R_a T + R_b \cdot \exp(-E_a/k_{\mathrm{B}}T), \quad (5)$$

a metallic-like contribution, which dominates at low temperatures. The coefficients R_0, R_a, R_b as well as the activation energy E_a are free parameters. R_0 a residual temperature independent resistance that we include in the metallic-like contribution only, provides a saturation of the resistance at low temperatures. The contribution $R_m(T)$ was already used to explain the

$R_M(\Omega)$	$T_{0,\mathrm{Mott}}(\mathrm{K})$	$R_0(\Omega)$	$R_a(\Omega)$
686.66	723.6	2431.31	20.08
$R_b(\Omega)$	$E_a(\mathrm{meV})$	$N(E_F)\ (\mathrm{eV}^{-1}\mathrm{cm}^{-1})$	
276.4	1.96	2.3×10^{24}	

TABLE I. Summary of parameters obtained after fitting the resistance $R_{A2}(T)$ using Eq. (4).

temperature dependence of the resistance in bulk graphite [24], few layer graphene samples [22, 25] and nano-graphite thin films [20]. Its origin is related to certain interfaces formed between the graphite crystallites. We can fit the experimental resistance data to Eq. (4) very well. The results are shown as continuous lines in Fig. 4 and the fitting parameters are listed in Table I.

The inset of Fig. 4 shows clearly the temperature ranges where each transport mechanism dominates the electric transport. We have assumed a localization length of $\xi \approx 0.5$ nm [26], which was estimated for similar samples, by means of spectroscopic ellipsometry, Raman spectroscopy and transport measurements. The localization length used in this work is close to the value of 1.2 nm used by Hauser et-al [2]. We estimate $N(E_F) \sim 2.3 \times 10^{24}$ $\mathrm{eV}^{-3}\mathrm{cm}^{-1}$, which is of the same order as reported for graphitic materials [27] and multi-walled carbon nanotubes [28]. Values of $N(E_F)$ of several orders of magnitude lower than our result were found for similar ion irradiated diamond, but these samples were not annealed [2, 29] or even measured when a barrier was present [29]. Finally, the calculated resistivity of the GLM is $\rho_{(300\ \mathrm{K})} = 7 \ldots 8 \times 10^{-5}$ Ωm, one order of magnitude larger than bulk graphite in-plane resistivity ($\rho_{(300\ \mathrm{K})} = 0.5 \times 10^{-5}$ Ωm) [21, 22, 30] or the resistivity of few layer graphene ($\rho_{(300\ \mathrm{K})} = 3 \ldots 50 \times 10^{-5}$ Ωm) [21, 22] and three orders of magnitude lower than pure amorphous carbon ($\rho_{(300\ \mathrm{K})} > 10^{-2}$ Ωm) [31, 32]. However, the GLM resistivity is comparable to other nano-graphite thin films prepared by chemical vapor deposition and aerosol assisted chemical vapor deposition ($\rho_{(300\ \mathrm{K})} = 3 \ldots 8 \times 10^{-5}$ Ωm) [20]. From experiments it is known that the resistivity ratio between the in-plane (ρ_a) and out-of-plane (ρ_c) resistivity in graphite is in the order of $\rho_c/\rho_a \approx 10^3 - 10^4$ [30, 33], indicating that the transport in our sample is dominated by the in-plane resistivity. Further, it means that the produced GLM have nano-crystals with a preferential c-axis normal to the substrate surface. The obtained transport characteristics of the produced GLM are important for future applications, because the resistivity and its temperature dependence make this GLM interesting to be used for electronic circuits in a broad temperature range.

3.3. Magnetoresistance

To obtain any information of the magnetic properties of the GLM there are no experimental methods other than transport because the wire is not only embedded inside the diamond matrix but also its mass is too small to be measured with commercial magnetometers. The magneto-transport measurements at different constant temperatures were done with an external magnetic field applied perpendicular to the current and main axis of the GLM. The results of the magnetoresistance MR defined as $MR = [R(B) - R(0)]/R(0)$ are shown in Fig. 5.

We observe a magnetic field dependence of the resistance, which is positive at $T = 2$ K, and negative in the field range of -3 T $< B <$ 3 T at 5 K and 10 K. At temperatures $T > 10$ K the MR is negative in all the field range. The positive MR at very low temperatures can be understood as a consequence of the strong Lorentz contribution. This tends to vanish at high temperatures. The negative MR can be attributed to a spin dependent scattering process. Due to the relatively high temperatures and magnetic field range where the negative MR is observed, we can rule out weak localization effects. According to the theory developed by

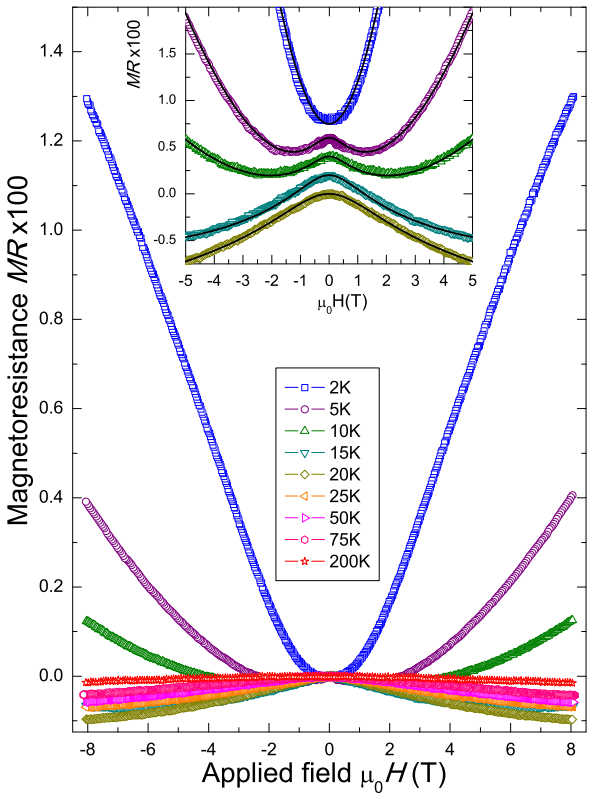

Fig. 5. Magnetoresistance at different constant temperatures. The inset shows the MR obtained at $T \leqslant 20$ K. The lines through the points are fits to Eq. (6). The results were shifted by a constant in the vertical axis in order to facilitate a detailed view.

Toyozawa [34] and later modified by Khosla and Fischer [35], the MR of systems with localized magnetic moments can be described using the following equation:

$$MR = -P_1^2 \ln(1 + P_2^2 B^2) + \frac{P_3^2 B^2}{1 + P_4^2 B^2}. \quad (6)$$

The free parameters P_1 and P_2 depend on several factors such as a spin scattering amplitude, the exchange integral, the density of states at the Fermi energy, the spin of the localized magnetic moments and the average magnetization square [34, 35]. The parameters P_3 and P_4 depend on the conductivity and the carrier mobility. In general, Eq. (6) contains two competitive terms. The first term describes the negative contribution due to a spin-dependent scattering mechanism (s-d usually in d-band ferromagnets, s-p in p-band ferromagnets [36]). The second term describes a positive MR due to the usual Lorentz force contribution. Using this equation we have fitted our experimental results. They are shown as continuous lines in the inset of Fig. 5 and the corresponding parameters are listed in Table II. The fits describe very well the experimental results at all measured temperatures, indicating the existence of spin dependent scattering in our GLM, however, this is not an evidence of magnetic order. Similar results were already observed in magnetic samples where the magnetic order was triggered by defects, as in proton irradiated graphite [37], proton irradiated ZnO:Li microwires [38], as well as in samples with magnetic elements like in single multi-walled carbon nanotubes filled with Fe nanorods [39].

$T(K)$	P_1	$P_2(1/\mathrm{K})$	$P_3(1/\mathrm{K})$	$P_4(1/\mathrm{K})$
2	0.1643	0.0300	0.02053	0.16316
5	0.013	1.68	0.00936	0.05081
10	0.0114	1.6428	0.00541	0.00133
15	0.0148	1.00675	0.0015	4.075E-7
20	0.017	0.668	1E-4	3.07E-7

TABLE II. Summary of parameters obtained after fitting the MR using Eq. (6).

The magnetic scattering contribution in our samples can be explained as a consequence of defects present in the disordered graphite structure of the microwire. Because of the preparation method used to produce the microwire, we can rule out the presence of magnetic impurities. The almost zero MR for temperatures $T \gtrsim 200$ K opens the possibility to use GLMs in a device under application of high magnetic fields.

4. CONCLUSION

In this work we have prepared a graphitized wire of 1350 μm length and lateral area of ≈ 15 μm × 130 nm inside a diamond matrix by means of He^+ irradiation and heat treatment. After annealing, the resistivity of the microwire is only one order of magnitude larger compared to graphite. Also, its temperature dependence can be well described by the parallel contribution of VRH and a metallic-like conduction, similar has been observed in other carbon based materials. The measured magnetoresistance can be well described by a semi empirical model, which takes into account a spin dependent transport mechanism used to describe the MR of magnetic diluted semiconductors as well as magnetic carbon-based materials, related to the defect-induced magnetism.

In summary, the low resistivity ($\rho_{(300\ \mathrm{K})} = 7 \ldots 8 \times 10^{-5}\Omega\mathrm{m}$), the small resistivity ratio ($\rho(2\mathrm{K})/\rho(315\mathrm{K}) \approx 1.275$) and the very small magnetoresistance, make the graphitized wires inside diamond candidates to be used as circuit elements. Our microwire preparation can be taken as basis for the production and future application of GLMs inside diamonds. For example, a GLM can be used to produce a magnetic field by a loop inside the diamond and thus allows, e.g., further manipulation of NV-centers for future application in quantum computation. Another possibility is the application in biology. Considering that diamond is a biocompatible material, the here used method would enable the design and production of complete electrical circuits that can allow the monitoring of electric signals *in-situ* the human body.

ACKNOWLEDGMENTS

We thank F. Bern for technical support in the magnetoresistance measurements.

[1] V. S. Vavilov, V. V. Krasnopevtsev, Y. V. Miljutin, A. E. Gorodestsky, and A. P. Zakharov, "On structural transitions in ion implanted diamond," Radiation Effects **22:2**, 141–143 (1974).

[2] J.J. Hauser, J.R. Patel, and J.W. Rodgers, "Hard conducting implanted diamond layers," Appl. Phys. Lett. **30**, 129–130 (1977).

[3] J.J. Hauser and J.R. Patel, "Hopping conductivity in c-implanted amorphous diamond, or how to ruin a perfectly good diamond," Solid State Commun. **18**, 789–790 (1976).

[4] F. Picollo, D. Gatto Monticone, P. Olivero, B.A. Fairchild, S. Rubanov, S. Prawer, and E. Vittone, "Fabrication and electrical characterization of three-dimensional graphitic microchannels in single crystal diamond," New Journal of Physics **14**, 053011 (2012).

[5] S. Talapatra, P. G. Ganesan, T. Kim, R. Vajtai, M. Huang, M. Shima, G. Ramanath, D. Srivastava, S. C. Deevi, and P. M. Ajayan, "Magnetic properties of point defects in proton irradiated diamond," Phys. Rev. Lett. **95**, 097201 (2005).

[6] T. N. Makgato, E. Sideras-Haddad, S. Shrivastava, M. Madhuku, K. Sekonya, A. Pineda-Vargas, and D. Joubert, "Magnetization effects in proton micro-irradiated diamond," arXiv:1409.2997.

[7] T. N. Makgato, E. Sideras-Haddad, M. A. Ramos, M. Garcia-Hernandez, A. Climent-Font, M. Munoz-Martin, A. Zucchiatti,

S. Shrivastava, and R. Erasmus, "Magnetic properties of point defects in proton irradiated diamond," J. Magn. Magn. Mat. **413**, 76–80 (2016).

[8] P. Esquinazi, W. Hergert, D. Spemann, A. Setzer, and A. Ernst, "Defect-induced magnetism in solids," Magnetics, IEEE Transactions on **49**, 4668–4674 (2013).

[9] D. Spemann, T. Reinert, J. Vogt, T. Butz, K. Otte, and K. Zimmer, "Novel test sample for submicron ion-beam analysis," Nucl. Instr. and Meth. B **181**, 186–192 (2001).

[10] D. J. W. Mous, R. G. Haitsma, T. Butz, R.-H. Flagmeyer, D. Lehmann, and J. Vogt, "The novel ultrastable hvee 3.5 mv singletron^{tm} accelerator for nanoprobe applications," Nucl. Instr. and Meth. B **130**, 31–36 (1997).

[11] C. Uzan-Saguy, C. Cytermann, R. Brener, V. Richter, M. Shaanan, and R. Kalish, "Damage threshold for ion-beam induced graphitization of diamond," Appl. Phys. Lett. **67**, 1194–1196 (1995).

[12] R. Kalish, A. Reznik, S. Prawer, D. Saada, and J. Adler, "Ion-implantation-induced defects in diamond and their annealing: experiment and simulation," Physica Status Solidi A-Applied Research **174**, 83–89 (1999).

[13] J. Ziegler, "The stopping and range of ions in matter," www.srim.org (2013).

[14] M. T. Robinson and I. M. Torrens, "Computer simulation of atomic-displacement cascades in solids in the binary-collision approximation," Phys. Rev. B **9**, 508–524 (1974).

[15] D. Saada, J. Adler, and R. Kalish, "Transformation of diamond (sp^3) to graphite (sp^2) bonds by ion-impact," Int. J. Mod. Phys. C **09**, 61 (1998).

[16] Z. Ma, J. Wu, W. Shen, L. Yan, X. Pan, and J. Wang, "Etching of CVD diamond films using oxygen ions in ECR plasma," Appl. Surf. Sci. **289**, 533–537 (2014).

[17] L. G. Cancado, K. Takai, T. Enoki, M. Endo, Y. A. Kim, H. Mizusaki, A. Jorio, L. N. Coelho, R. Magalhaes-Paniago, and M. A. Pimenta, "General equation for the determination of the crystallite size L_a of nanographite by raman spectroscopy," Appl. Phys. Lett. **88**, 163106–3 (2006).

[18] S. Rubanov, B. A. Fairchild, A. Suvorova, P. Olivero, and S. Prawer, "Structural transformation of implanted diamond layers during high temperature annealing," Nucl. Instr. and Meth. B **365**, 5054 (2015).

[19] J. Barzola-Quiquia, P. Esquinazi, M. Lindel, D. Spemann, M. Muallem, and G.D. Nessim, "Magnetic order and superconductivity observed in bundles of double-wall carbon nanotubes," Carbon **88**, 16–25 (2015).

[20] J. L. Cholula-Diaz, J. Barzola-Quiquia, H. Krautscheid, U. Teschner, and P. Esquinazi, "Synthesis and magnetotransport properties of nanocrystalline graphite prepared by aerosol assisted chemical vapor deposition," Carbon **67**, 10–16 (2014).

[21] J. Barzola-Quiquia, J.-L. Yao, P. Rödiger, K. Schindler, and P. Esquinazi, "Sample

size effects on the transport characteristics of mesoscopic graphite samples," Phys. Stat. Sol. (a) **205**, 2924–2933 (2008).

[22] M. Zoraghi, J. Barzola-Quiquia, M. Stiller, A. Setzer, P. Esquinazi, G. H. Kloess, T. Muenster, T. Lühmann, and I. Estrela-Lopis, "Influence of rhombohedral stacking order in the electrical resistance of bulk and mesoscopic graphite," Phys. Rev. B **95**, 045308 (2017).

[23] N. F. Mott, "Conduction in glasses containing transition metal ions," J. Non-Cryst. Solids **1**, 1–17 (1968).

[24] K. Matsubara, K. Sugihara, and T. Tsuzuku, "Electrical resistance in the c direction of graphite," Phys. Rev. B **41**, 969–974 (1990).

[25] N. Garcia, P. Esquinazi, J. Barzola-Quiquia, and S. Dusari, "Evidence for semiconducting behavior with a narrow band gap of Bernal graphite," New Journal of Physics **14**, 053015 (14pp) (2012).

[26] T. Lühmann, *3D Ionenstrahlschreiben in Diamant zur Erzeugung von Graphitstrukturen und deren Charakterisierung*, Master's thesis, University Leipzig, Germany (2015).

[27] K. G. Raj and P. A. Joy, "Cross over from 3D variable range hopping to the 2D weak localization conduction mechanism in disordered carbon with the extent of graphitization," Phys. Chem. Chem. Phys. **17**, 16178–16185 (2015).

[28] Z. H. Khan, M. Husain, T. P. Perng, N. Salah, and S. Habib, "Electrical transport via variable range hopping in an individual multi-wall carbon nanotube," J. Phys.: Condens. Matter **20**, 475207 (7pp) (2008).

[29] P. Olivero, G. Amato, F. Bellotti, S. Borini, A. Lo Giudice, F. Picollo, and E. Vittone, "Direct fabrication and iv characterization of sub-surface conductive channels in diamond with mev ion implantation," Eur. Phys. J. B **75**, 127132 (2010).

[30] H. Kempa, P. Esquinazi, and Y. Kopelevich, "Field-induced metal-insulator transition in the c-axis resistivity of graphite," Phys. Rev. B **65**, 241101(R) (2002).

[31] A. Grill, "Electrical and optical properties of diamond-like carbon," Thin Solid Films **355356**, 189193 (1999).

[32] J.J. Hauser, "Hopping conductivity in amorphous carbon films," Solid State Commun. **17**, 1577–1580 (1975).

[33] Y. Kopelevich, J. H. S. Torres, R. R. da Silva, F. Mrowka, H. Kempa, and P. Esquinazi, "Reentrant metallic behavior of graphite in the quantum limit," Phys. Rev. Lett. **90**, 156402–1–4 (2003).

[34] Y. Toyozawa, "Theory of localized spins and negative magnetoresistance in the metallic impurity conduction," J. Phys. Soc. Japan **17**, 986–1004 (1962).

[35] R. Khosla and J. Fischer, "Magnetoresistance in degenerate CdS: Localized magnetic moments," Phys. Rev. B **2**, 4084–4097 (1970).

[36] O. Volnianska and P. Boguslawski, "Magnetism of solids resulting from spin polar-

ization of p orbitals," J Phys: Condens Matter **22**, 073202 (19pp) (2010).

[37] P. Esquinazi, J. Barzola-Quiquia, D. Spemann, M. Rothermel, H. Ohldag, N. García, A. Setzer, and T. Butz, "Magnetic order in graphite: Experimental evidence, intrinsic and extrinsic difficulties," J. Magn. Magn. Mat. **322**, 1156–1161 (2010).

[38] I. Lorite, C. Zandalazini, P. Esquinazi, D. Spemann, S. Friedländer, A. Pöppl, T. Michalsky, M. Grundmann, J. Vogt, J. Meijer, S.P. Heluani, H. Ohldag, W.A. Adeagbo, S.K. Nayak, W. Hergert, A. Ernst, and M. Hoffmann, "Study of the negative magneto-resistance of single proton-implanted lithium-doped ZnO microwires," J. Phys.: Condens. Matter **27**, 256002 (2015).

[39] J. Barzola-Quiquia, N. Klingner, J. Krüger, A. Molle, P. Esquinazi, A. Leonhardt, and M. T. Martinez, "Quantum oscillations and ferromagnetic hysteresis observed in iron filled multiwall carbon nanotubes," Nanotechnology **23**, 015707 7(pp) (2012).